Large effects of subtle electronic correlations on the energetics of vacancies in α-Fe

Pascal Delange,[1] Thomas Ayral,[2] Sergei I. Simak,[3] Michel Ferrero,[1,4] Olivier Parcollet,[2]
Silke Biermann,[1,4] and Leonid Pourovskii[1,4,5]

[1]*Centre de Physique Théorique, École Polytechnique, CNRS, Université Paris-Saclay, 91128 Palaiseau Cedex, France*
[2]*Institut de Physique Théorique (IPhT), CEA, CNRS, UMR 3681, 91191 Gif-sur-Yvette, France*
[3]*Department of Physics, Chemistry and Biology (IFM), Linköping University, SE-58183 Linköping, Sweden*
[4]*Collège de France, 11 place Marcelin Berthelot, 75005 Paris, France*
[5]*Materials Modeling and Development Laboratory, National University of Science and Technology "MISIS," Moscow, Russia*

We study the effect of electronic Coulomb correlations on the vacancy formation energy in paramagnetic α-Fe within *ab initio* dynamical mean-field theory. The calculated value for the formation energy is substantially lower than in standard density-functional calculations and in excellent agreement with experiment. The reduction is caused by an enhancement of electronic correlations at the nearest neighbors of the vacancy. This effect is explained by subtle changes in the corresponding spectral function of the *d* electrons. The local lattice relaxations around the vacancy are substantially increased by many-body effects.

Point defects, such as vacancies, play an important role for the mechanical and thermodynamic properties of materials [1]. However, the experimental determination of vacancy formation or migration energies is difficult. Even the best available techniques, the differential dilatometry and the positron annihilation spectroscopy, suffer from large error bars, and the discrepancies between different measurements on one and the same material may be significant. Therefore, *ab initio* theoretical calculations are an indispensable tool for developing a better understanding of the defect properties of materials [2].

Early density-functional theory (DFT) calculations in the local density approximation (LDA) have predicted formation energies of vacancies in simple metals in good agreement with experiment [3,4]. Despite a large body of successful calculations, it has later been recognized that the nice agreement with experiment could often be the effect of the cancellation of errors in the exchange and correlation parts of the density functional [5]. As has been discussed by Ruban [6], despite the structural simplicity of vacancies, their energetics is still one of the least reliable physical properties determined in first-principles calculations.

In transition metals, where the open *d* shells are often poorly described in LDA or the generalized gradient approximation (GGA), the quality of results of DFT calculations for point defect properties is rather unpredictable and strongly material dependent. There have been several attempts to improve the available functionals (see, e.g., Refs. [7–10]). We notice that the predicted vacancy formation energies seem to be especially poor for 3*d* transition metals, for which many-body effects are fairly important, in particular in the paramagnetic state and body-centered cubic (bcc) crystal structure [11]. Likewise, DFT has limitations for point defect calculations in correlated lanthanide or actinide oxides with 4*f* or 5*f* electrons, for example in the case of uranium oxides used in the nuclear industry [12].

Among the 3*d* transition metals, iron is a particularly complex system, where the strength of electronic correlations is very sensitive to the lattice structure and magnetic state. However, from a practical point of view, vacancies in iron and steels are of particular interest because they affect a number of important characteristics of the metal, e.g., toughness and ductility. Iron's low-temperature ferromagnetic bcc α phase is a weakly renormalized Fermi liquid [13] well described within DFT [14–16]. However, the same α-Fe in the high-temperature paramagnetic phase exhibits a strongly correlated non-Fermi-liquid behavior [17–19] with DFT calculations failing to describe its structural parameters (lattice constants, bulk modulus, or even the shape of the crystal) [18]. The low-temperature paramagnetic hexagonal ε phase stabilized by pressure is also rather strongly correlated [13] (though less so as compared to paramagnetic α-Fe), exhibiting a large electron-electron scattering contribution to the resistivity [20] as well as unconventional superconductivity [21,22]. All this hints at a strong sensitivity of many-body effects in Fe to local disturbances of the crystalline order (e.g., to point defects) that cannot be captured easily within standard DFT. Indeed, extensive DFT calculations of α-Fe [23–34] predict a monovacancy formation energy about 30%–40% higher than the measured values, with significant scatter depending on the DFT implementation used (see also Table II in Ref. [35]). In contrast to other 3*d* metals, this formation energy has been somewhat reliably determined thanks to extensive experiments [36–40].

The deficiencies of standard DFT to describe ε-Fe and paramagnetic α-Fe have been successfully corrected by combining it with a dynamical mean-field theory (DMFT) [41,42] treatment of the local repulsion between 3*d* electrons. *Ab initio* calculations using this DFT+DMFT approach [43,44] were able to reproduce the ground-state properties and phonon spectra of the α and δ phase [18,45,46] as well as the equation of state of ε-Fe [13]. It is thus likely that an explicit treatment of many-body effects within DMFT will also correct the severe problems of DFT in describing point defects in iron.

Hence, in the present work we have developed the state-of-the-art DFT+DMFT method [47–50] into a scheme for studying vacancy properties. We have applied our technique to a single vacancy in paramagnetic α-Fe, where positron annihilation measurements have been performed on pure iron without further approximations (contrary to the formation energy in

(a) $2 \times 2 \times 2$ supercell   (b) $3 \times 3 \times 3$ supercell
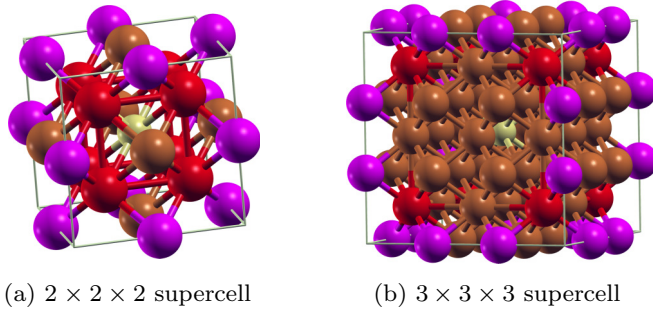
FIG. 1. The $2 \times 2 \times 2$ and $3 \times 3 \times 3$ supercells with the vacancy in the corner. Different colors indicate the atom nearest to the vacancy (red), the second nearest (purple), and the furthest (the central atom, yellow). Generated with XCRYSDEN [52].

FIG. 2. Vacancy formation energies calculated by different methods (GGA and DFT+DMFT) in the different setups: small and large supercell, relaxed or not, nonmagnetic, paramagnetic (PM) or ferromagnetic (FM). Calculations are performed at the equilibrium volume for the relevant setup. The average of experimental values is shown for comparison [36–40].

the ferromagnetic phase). We have computed the electronic structure around the vacancy as well as the vacancy's formation energy, taking into account local lattice distortions around the defect. We do not treat here the high-temperature face-centered cubic phase, or temperatures close to the melting point, where the influence of the (anharmonic) lattice vibrations may play a crucial role [5,10,51] and the bcc phase is stabilized again. Compared to ferromagnetic DFT calculations, a significant reduction of the theoretical formation energy is obtained, with calculated values in remarkable agreement with experimental estimates [36–40]. We trace back this reduction to rather subtle effects of the vacancy on the local density of states and hybridization with its nearest neighbors.

We model a single vacancy in bcc Fe using the $2 \times 2 \times 2$ and $3 \times 3 \times 3$ cubic supercells represented in Fig. 1, with the vacancy placed at the origin of the supercells. We compute the vacancy formation energy from the supercell total energy using the standard formula

$$E_{\text{vac}}^{f} = E^{\text{vac}}(N-1) - \frac{N-1}{N} E^{\text{no vac}}(N), \quad (1)$$

where N is the number of atoms in the ideal supercell, $E^{\text{no vac}}(N)$ is the total energy of the ideal supercell containing N atoms and no vacancy, and $E^{\text{vac}}(N-1)$ is the total energy of the same supercell with a vacancy (hence $N-1$ atoms). N is 16 in the $2 \times 2 \times 2$ supercell and 54 in the $3 \times 3 \times 3$ supercell, corresponding to vacancy concentrations of 6.25% and 1.85%, respectively.

Our calculations have been carried out using a fully charge self-consistent implementation of DFT+DMFT [53,54] based on the TRIQS package [55,56], with LDA as DFT exchange-correlation potential. This implementation is based on the full potential linearized augmented plane-wave WIEN2K code [57]. The on-site density-density interaction between those orbitals is parametrized by the Slater parameter $F_0 = U = 4.3$ eV and the Hund's rule coupling $J = 1.0$ eV that were previously used in the DFT+DMFT calculations of α and ϵ-Fe of Ref. [13]. The same work reproduced almost exactly the experimental lattice parameter of 2.86 Å, hence we perform our DFT+DMFT calculations at the experimental volume. Other DFT calculations were performed at the corresponding theoretical volume. Technical details about the DFT and DFT+DMFT calculations are included in the Supplemental

Material [35]. The calculation of a vacancy formation energy using supercells with seven inequivalent atomic sites has become possible thanks to the use of a continuous-time quantum Monte Carlo hybridization expansion algorithm [58] in the segment representation for the solution of the local impurity problems (Backes *et al.* (Ref. [59]) and Behrmann *et al.* (Ref. [60]) have reported about the effect of vacancies on magnetism within DFT+DMFT). All DFT+DMFT calculations were performed at a temperature of 1162 K.

The vacancy formation energies obtained within DFT+DMFT together with different DFT results and experimental values are shown in Fig. 2 (see also Table I of the Supplemental Material [35]). The resulting value for E_{vac}^{f} in DFT+DMFT is 1.77 eV for the unrelaxed 54-atom supercell with lattice relaxations reducing it further to $E_{\text{vac}}^{f} = 1.56 \pm 0.13$ eV, in excellent agreement with the mean experimental value of about 1.6 eV. We also calculated E_{vac}^{f} within DFT+DMFT for the unrelaxed ferromagnetic phase obtaining a higher value of 2.45 ± 0.15 eV. Experiments indeed seem to confirm that E_{vac}^{f} in the ferromagnetic phase should be larger than in the nonmagnetic one [39,40], although direct low-temperature measurements of E_{vac}^{f} in the ferromagnetic phase with positron annihilation spectroscopy are notoriously difficult.

DFT (GGA) calculations assuming ferromagnetic bcc Fe predict a significantly larger value E_{vac}^{f} of 2.51 and 2.32 eV for an unrelaxed and a fully relaxed cell, respectively. Hence, one sees that many-body effects included within DMFT reduce E_{vac}^{f} for the paramagnetic phase by about 0.7 eV. The impact of correlation effects for ferromagnetic α-Fe is much less significant, in agreement with the predicted suppression of dynamic correlations in this phase [13]. Indeed, the large static spin splitting in the ferromagnetic phase leads to a suppression of dynamical correlations, which explains
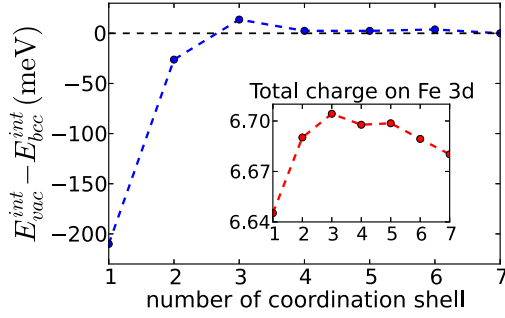
FIG. 3. Difference in the interaction energy per atom, before and after adding a vacancy. Inset: Fe $3d$ charge in the cell with vacancy.

why DFT works well in the ferromagnetic, but not in the paramagnetic phase of α-Fe. The vacancy formation energies obtained with nonmagnetic DFT calculations are even lower than the measured values, with $E_{\text{vac}}^{f} \approx 1.5$ eV in unrelaxed GGA. They have, however, very little physical meaning: DFT in general fails dramatically for the paramagnetic phase, which is reflected by the fact that α-Fe is not dynamically stable and the predicted lattice parameter would be significantly smaller in nonmagnetic DFT. Hence, using our relaxed positions in a nonmagnetic DFT calculation gives an (unphysical) negative vacancy formation energy. Thus, the strongly reduced value of E_{vac}^{f} in nonmagnetic DFT calculations compared to ferromagnetic ones may be due to a spurious cancellation of errors.

The total energy in DFT+DMFT is

$$E_{\text{DMFT}}^{\text{tot}} = \text{Tr}\left(\hat{\epsilon}_k \hat{\rho}_k^{\text{DMFT}}\right) + E[\rho^{\text{DMFT}}] + (E_{\text{Hub}} - E_{\text{DC}}), \quad (2)$$

where $\hat{\rho}_k^{\text{DMFT}}$ is the density matrix for crystal momentum k, $\hat{\epsilon}_k$ the corresponding LDA Hamiltonian and $E[\rho^{\text{DMFT}}]$ only depends explicitly on the charge density. $E_{\text{Hub}} = \frac{1}{2} \sum_{ij} U_{ij} \langle n_i n_j \rangle$ is the Coulomb interaction between Fe $3d$ electrons (i and j are orbital indices and U_{ij} is the density-density Coulomb matrix), and E_{DC} is the double-counting term that estimates the energy already present in LDA (see Supplemental Material for the details [35]). When one removes an atom from the cell to create a vacancy, all three terms in Eq. (2) change. Figure 3 shows the difference in the third term, $E^{\text{int}} = E_{\text{Hub}} - E_{\text{DC}}$, on each respective atom of the supercell before and after removing an atom. Summing this up and taking into account the multiplicity of the atoms in the cell yields a change $\Delta E^{\text{int}} \approx -1.6$ eV, that is compensated by a larger change in $E[\rho^{\text{DMFT}}]$ due to a redistribution of the charge density, as wave functions from DFT+DMFT are more localized. The contributions from the second and third coordination shells compensate one another, so that the net change in the interaction energy only comes from the first nearest neighbor. This is due to good metallic screening, and is in good agreement with embedded atom method calculations of iron vacancies near a surface [61] that show the vacancy formation energy becomes equal to the bulk value for the vacancy located in the third layer or deeper.

The self-energy of the vacancy's first coordination shell shows a significant difference from the bulk bcc-Fe self-energy, as shown in Figs. 4(a) and 4(b). t_{2g} states, but also e_g states to a lesser extent, become more strongly correlated
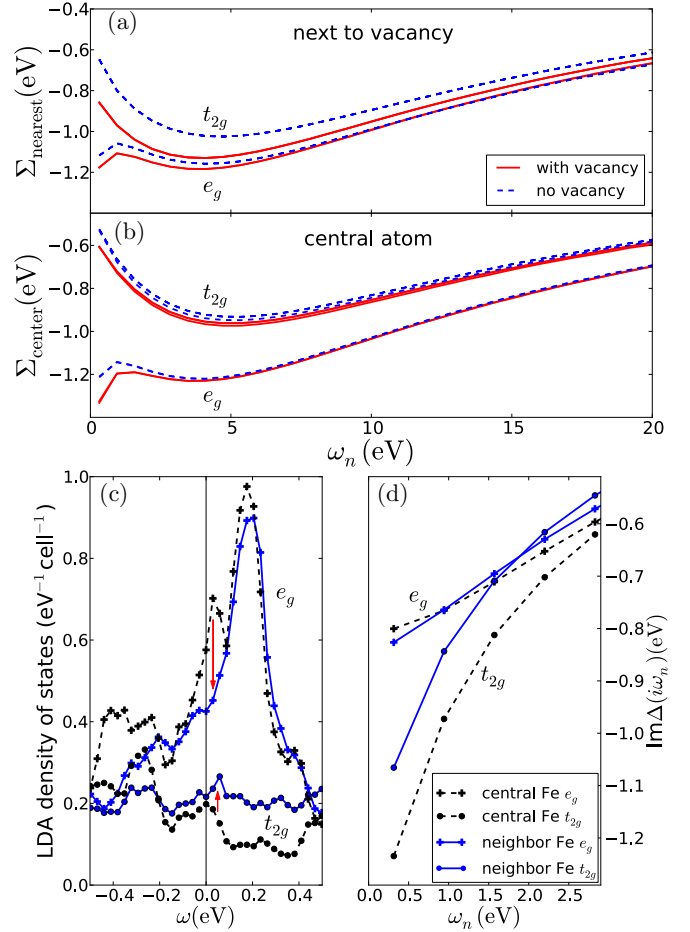
FIG. 4. Imaginary part of the Matsubara self-energies for (a) the vacancy nearest neighbor and (b) central atom in the $3 \times 3 \times 3$ supercell with a vacancy present (red, full) or without it (blue, dashed). Correlations become stronger on the atom nearest to the vacancy, while the difference between e_g and t_{2g} is strongly reduced. (c) LDA density of states around the Fermi level and (d) hybridization function on the Matsubara axis for the nearest neighbors (blue, full) to the vacancy, and for the central atom (black, dashed). The full Fe $3d$ DOS is shown in the Supplemental Material [35].

(less coherent) with a larger $\text{Im}\Sigma(i\omega)$. A larger absolute value of the imaginary part of the self-energy at low frequencies means a shorter quasiparticle lifetime, synonymous to stronger dynamic correlations. This difference almost vanishes for the self-energy of the atoms further than the nearest neighbor, in agreement with the variation of the interaction energy shown in Fig. 3. Stronger correlations on the atoms near the vacancy imply that a more correct description of the $3d$ electrons of the Fe atoms in DFT+DMFT, already important to predict the crystal structure and lattice parameter, is especially crucial when estimating the energetics of the vacancy and indeed leads to a smaller formation energy. Note that the self-energies are slightly atom dependent even in the absence of a vacancy in our calculations, due to an artificial symmetry breaking in the supercell in DFT calculations and the nonrotational invariance of the density-density Hubbard Hamiltonian. However, we compare self-energies and interaction energies in a consistent, atom-to-atom way.

The enhancement of the nearest-neighbor self-energy can be traced back to a change in the hybridization function. As can be seen in Fig. 4(d), the imaginary-frequency hybridization function, in particular for the t_{2g} states, is reduced at low frequencies for the atom near the vacancy. This reduction is due to an increase in the corresponding t_{2g} partial density of states (DOS) in the vicinity of the Fermi level, E_F, as one can see in Fig. 4(c). A larger DOS at E_F induces a suppression of low-energy hopping leading to stronger correlation [19,62]: at the first iteration of DMFT, $\mathrm{Im}\Delta(i0^+) = -\pi\rho_F/[\mathrm{Re}G_{\mathrm{loc}}(i0^+)^2 + (\pi\rho_F)^2] \approx -1/(\pi\rho_F)$, with ρ_F the LDA DOS. The enhancement of the nearest-neighbor e_g self-energy is smaller and the corresponding DOS at E_F even decreases compared to the bulk case. This decrease in the value of the DOS exactly at E_F is compensated by an overall narrowing of the e_g peak in the vicinity of E_F [see Fig. 4(c)]. Hence, the resulting hybridization function for e_g is still suppressed starting from the second Matsubara point.

Next, we calculated the relaxed atomic positions in DFT+DMFT around the vacancy. Computing atomic forces in DFT+DMFT is rather complicated [63], so we obtained the relaxed atomic positions by moving atoms and minimizing the total energies. We performed a relaxation of the atoms around the vacancy in two steps, in order to reduce the computational effort. We first performed the full relaxation in spin-polarized GGA (at its corresponding theoretical volume, computing atomic forces), to obtain an initial guess of the atomic positions. We observe a shift of the first coordination shell towards the vacancy by about 4%, and a shift of the second coordination shell away from the vacancy by about 1.5%, while all the other atoms do not move significantly, in agreement with previous calculations [25]. In the second step, the positions of the two first nearest neighbors were relaxed within DFT+DMFT. In Fig. 5 we show the total energy (minus an offset depending on the method used, GGA or DFT+DMFT) of the supercell as a function of the relaxed position of the nearest and second nearest neighbor of the vacancy. Each site was moved independently, preserving the symmetry of the cell, while the positions of others were fixed at their fractional GGA values. We obtain the following results: in DFT+DMFT, for paramagnetic α-Fe, the first nearest neighbor relaxes by 5.7% towards the vacancy, while the second nearest neighbor relaxes away from it by 0.7%. One sees that many-body effects have a significant impact on the nearest-neighbor relaxation, enhancing it by almost 50%. Overall, relaxing the two first coordination shells in full DFT+DMFT reduces the vacancy formation energy by 0.21 eV.

In conclusion, we have shown that local many-body effects are crucial for explaining a relatively low vacancy formation energy in α-Fe. The presence of a vacancy induces rather subtle changes in the local electronic structure of its surroundings, leading to a moderate increase in the strength of correlations at neighboring sites. This moderate increase has, however, a
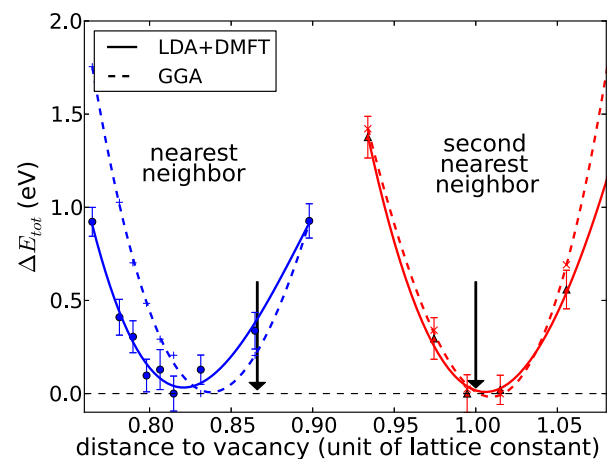
FIG. 5. Total energy vs distance to the vacancy (as a fraction of the lattice parameter) for the first nearest neighbor (blue) and the second nearest neighbor (red), in DFT+DMFT (full line) and GGA (dashed line). The black arrows show the position of the atoms in the unrelaxed bcc supercell.

very significant impact on the vacancy energetics. When the effect of local relaxations is included, the calculated vacancy formation energy is reduced by about 0.7 eV compared with the corresponding DFT value and is in excellent agreement with experiment. The predicted magnitude of nearest-neighbor relaxations is about 50% larger compared to the one obtained within DFT. This remarkable sensitivity to correlation effects is most probably pertinent to other types of defects in iron that are of the crucial importance for mechanical properties and thermodynamics of steels, e.g., interstitial sites, stacking faults, and dislocations.

[1] W. D. Callister and D. G. Rethwisch, *Materials Science and Engineering: An Introduction* (Wiley, New York, 2007), Vol. 7.

[2] C. Freysoldt, B. Grabowski, T. Hickel, J. Neugebauer, G. Kresse, A. Janotti, and C. G. Van de Walle, Rev. Mod. Phys. **86**, 253 (2014).

[3] M. Manninen, P. Hautojärvi, and R. Nieminen, Solid State Commun. **23**, 795 (1977).

[4] B. Chakraborty, R. W. Siegel, and W. E. Pickett, Phys. Rev. B **24**, 5445 (1981).

[5] K. Carling, G. Wahnström, T. R. Mattsson, A. E. Mattsson, N. Sandberg, and G. Grimvall, Phys. Rev. Lett. **85**, 3862 (2000).

[6] A.V. Ruban, Phys. Rev. B **93**, 134115 (2016).

[7] R. Armiento and A. E. Mattsson, Phys. Rev. B **72**, 085108 (2005).

[8] A. E. Mattsson, R. R. Wixom, and R. Armiento, Phys. Rev. B **77**, 155211 (2008).

[9] R. Nazarov, T. Hickel, and J. Neugebauer, Phys. Rev. B **85**, 144118 (2012).

[10] A. Glensk, B. Grabowski, T. Hickel, and J. Neugebauer, Phys. Rev. X **4**, 011018 (2014).

[11] T. Korhonen, M. J. Puska, and R. M. Nieminen, Phys. Rev. B **51**, 9526 (1995).

[12] B. Dorado, M. Freyss, B. Amadon, M. Bertolus, G. Jomard, and P. Garcia, J. Phys.: Condens. Matter **25**, 333201 (2013).

[13] L. V. Pourovskii, J. Mravlje, M. Ferrero, O. Parcollet, and I. A. Abrikosov, Phys. Rev. B **90**, 155120 (2014).

[14] V. L. Moruzzi, P. M. Marcus, K. Schwarz, and P. Mohn, Phys. Rev. B **34**, 1784 (1986).

[15] L. Stixrude, R. E. Cohen, and D. J. Singh, Phys. Rev. B **50**, 6442 (1994).

[16] P. Söderlind, J. A. Moriarty, and J. M. Wills, Phys. Rev. B **53**, 14063 (1996).

[17] A. A. Katanin, A. I. Poteryaev, A. V. Efremov, A. O. Shorikov, S. L. Skornyakov, M. A. Korotin, and V. I. Anisimov, Phys. Rev. B **81**, 045117 (2010).

[18] I. Leonov, A. I. Poteryaev, V. I. Anisimov, and D. Vollhardt, Phys. Rev. Lett. **106**, 106405 (2011).

[19] L. V. Pourovskii, T. Miyake, S. I. Simak, A. V. Ruban, L. Dubrovinsky, and I. A. Abrikosov, Phys. Rev. B **87**, 115130 (2013).

[20] D. Jaccard and A. T. Holmes, Phys. B (Amsterdam, Neth.) **359-361**, 333 (2005).

[21] K. Shimizu, T. Kimura, S. Furomoto, K. Takeda, K. Kontani, Y. Onuki, and K. Amaya, Nature (London) **412**, 316 (2000).

[22] I. I. Mazin, D. A. Papaconstantopoulos, and M. J. Mehl, Phys. Rev. B **65**, 100511 (2002).

[23] P. A. Korzhavyi, I. A. Abrikosov, B. Johansson, A. V. Ruban, and H. L. Skriver, Phys. Rev. B **59**, 11693 (1999).

[24] P. Söderlind, L. H. Yang, J. A. Moriarty, and J. M. Wills, Phys. Rev. B **61**, 2579 (2000).

[25] C. Domain and C. S. Becquart, Phys. Rev. B **65**, 024103 (2001).

[26] T. Hoshino, T. Mizuno, M. Asato, and H. Fukushima, Mater. Trans. **42**, 2206 (2001).

[27] T. Mizuno, M. Asato, T. Hoshino, and K. Kawakami, J. Magn. Magn. Mater. **226**, 386 (2001).

[28] Y. Tateyama and T. Ohno, Phys. Rev. B **67**, 174105 (2003).

[29] C.-C. Fu, F. Willaime, and P. Ordejón, Phys. Rev. Lett. **92**, 175503 (2004).

[30] P. M. Derlet, D. Nguyen-Manh, and S. L. Dudarev, Phys. Rev. B **76**, 054107 (2007).

[31] P. Olsson, C. Domain, and J. Wallenius, Phys. Rev. B **75**, 014110 (2007).

[32] T. Ohnuma, N. Soneda, and M. Iwasawa, Acta Mater. **57**, 5947 (2009).

[33] D. Kandaskalov, C. Mijoule, and D. Connétable, J. Nucl. Mater. **441**, 168 (2013).

[34] S. Dudarev, Mater. Res. **43**, 35 (2013).

[35] See Supplemental Material at http://link.aps.org/supplemental/10.1103/PhysRevB.94.100102 for details on the DFT and DMFT methodology, as well as an extensive overview of our and other groups' theoretical and experimental results.

[36] H.-E. Schaefer, K. Maier, M. Weller, D. Herlach, A. Seeger, and J. Diehl, Scr. Metall. **11**, 803 (1977).

[37] S. Kim and W. Buyers, J. Phys. F **8**, L103 (1978).

[38] H. Matter, J. Winter, and W. Triftshäuser, Appl. Phys. **20**, 135 (1979).

[39] L. De Schepper, D. Segers, L. Dorikens-Vanpraet, M. Dorikens, G. Knuyt, L. M. Stals, and P. Moser, Phys. Rev. B **27**, 5257 (1983).

[40] H.-E. Schaefer, Phys. Status Solidi A **102**, 47 (1987).

[41] A. Georges, G. Kotliar, W. Krauth, and M. J. Rozenberg, Rev. Mod. Phys. **68**, 13 (1996).

[42] G. Kotliar and D. Vollhardt, Phys. Today **57** (3), 53 (2004).

[43] V. Anisimov, A. Poteryaev, M. Korotin, A. Anokhin, and G. Kotliar, J. Phys.: Condens. Matter **9**, 7359 (1997).

[44] A. I. Lichtenstein and M. I. Katsnelson, Phys. Rev. B **57**, 6884 (1998).

[45] I. Leonov, A. I. Poteryaev, V. I. Anisimov, and D. Vollhardt, Phys. Rev. B **85**, 020401 (2012).

[46] I. Leonov, A. Poteryaev, Y. N. Gornostyrev, A. Lichtenstein, M. Katsnelson, V. I. Anisimov, and D. Vollhardt, Sci. Rep. **4**, 5585 (2014).

[47] G. Kotliar, S. Y. Savrasov, K. Haule, V. S. Oudovenko, O. Parcollet, and C. Marianetti, Rev. Mod. Phys. **78**, 865 (2006).

[48] S. Biermann, in *Electronic Structure of Transition Metal Compounds: DFT-DMFT Approach*, edited by K. H. Jürgen Buschow, R. W. Cahn, M. C. Flemings, B. Ilschner (print), and E. J. Kramer, S. Mahajan, P. Veyssire (updates), Encyclopedia of Materials: Science and Technology (Elsevier, Oxford, 2006), pp. 1–9.

[49] F. Lechermann, A. Georges, A. Poteryaev, S. Biermann, M. Posternak, A. Yamasaki, and O. K. Andersen, Phys. Rev. B **74**, 125120 (2006).

[50] V. I. Anisimov, D. E. Kondakov, A. V. Kozhevnikov, I. A. Nekrasov, Z. V. Pchelkina, J. W. Allen, S.-K. Mo, H.-D. Kim, P. Metcalf, S. Suga *et al.*, Phys. Rev. B **71**, 125119 (2005).

[51] D. A. Andersson and S. I. Simak, Phys. Rev. B **70**, 115108 (2004).

[52] A. Kokalj, Comput. Mater. Sci. **28**, 155 (2003).

[53] M. Aichhorn, L. Pourovskii, V. Vildosola, M. Ferrero, O. Parcollet, T. Miyake, A. Georges, and S. Biermann, Phys. Rev. B **80**, 085101 (2009).

[54] M. Aichhorn, L. Pourovskii, and A. Georges, Phys. Rev. B **84**, 054529 (2011).

[55] O. Parcollet, M. Ferrero, T. Ayral, H. Hafermann, I. Krivenko, L. Messio, and P. Seth, Comput. Phys. Commun. **196**, 398 (2015).

[56] M. Aichhorn, L. Pourovskii, P. Seth, V. Vildosola, M. Zingl, O. E. Peil, X. Deng, J. Mravlje, G. J. Kraberger, C. Martins *et al.*, Comput. Phys. Commun. **204**, 200 (2016).

[57] P. Blaha, K. Schwarz, G. Madsen, D. Kvasnicka, and J. Luitz, *WIEN2k, An Augmented Plane Wave + Local Orbitals Program*

for Calculating Crystal Properties (Karlheinz Schwarz, Techn. Universität Wien, Austria, 2001).

[58] E. Gull, A. J. Millis, A. I. Lichtenstein, A. N. Rubtsov, M. Troyer, and P. Werner, Rev. Mod. Phys. **83**, 349 (2011).

[59] S. Backes, T. C. Rödel, F. Fortuna, E. Frantzeskakis, P. Le Fèvre, F. Bertran, M. Kobayashi, R. Yukawa, T. Mitsuhashi, M. Kitamura *et al.*, arXiv:1602.06909.

[60] M. Behrmann and F. Lechermann, Phys. Rev. B **92**, 125148 (2015).

[61] C. Wang, Y. Yang, Y. Zhang, and Y. Jia, Comput. Mater. Sci. **50**, 291 (2010).

[62] J. Mravlje, M. Aichhorn, T. Miyake, K. Haule, G. Kotliar, and A. Georges, Phys. Rev. Lett. **106**, 096401 (2011).

[63] I. Leonov, V. I. Anisimov, and D. Vollhardt, Phys. Rev. Lett. **112**, 146401 (2014).